

Influence of graphene-substrate interactions on configurations of organic molecules on graphene: Pentacene/epitaxial graphene/SiC

W. Jung, D.-H. Oh, I. Song, H.-C. Shin, S. J. Ahn, Y. Moon, C.-Y. Park, and J. R. Ahn

Citation: [Applied Physics Letters](#) **105**, 071606 (2014); doi: 10.1063/1.4893880

View online: <http://dx.doi.org/10.1063/1.4893880>

View Table of Contents: <http://scitation.aip.org/content/aip/journal/apl/105/7?ver=pdfcov>

Published by the [AIP Publishing](#)

Articles you may be interested in

[Graphene as a surfactant for metal growth on solid surfaces: Fe on graphene/SiC\(0001\)](#)

Appl. Phys. Lett. **104**, 181604 (2014); 10.1063/1.4875799

[Direct experimental evidence for the reversal of carrier type upon hydrogen intercalation in epitaxial graphene/SiC\(0001\)](#)

Appl. Phys. Lett. **104**, 041908 (2014); 10.1063/1.4863469

[Hafnium intercalation between epitaxial graphene and Ir\(111\) substrate](#)

Appl. Phys. Lett. **102**, 093106 (2013); 10.1063/1.4793427

[Direct imaging of intrinsic molecular orbitals using two-dimensional, epitaxially-grown, nanostructured graphene for study of single molecule and interactions](#)

Appl. Phys. Lett. **99**, 153101 (2011); 10.1063/1.3646406

[Epitaxial graphene on cubic SiC\(111\)/Si\(111\) substrate](#)

Appl. Phys. Lett. **96**, 191910 (2010); 10.1063/1.3427406



Automate your set-up with
Miniature Linear Actuators

Affordable. Built-in controllers.
Easy to set up. Simple to use.

ZABER

www.zaber.com



Influence of graphene-substrate interactions on configurations of organic molecules on graphene: Pentacene/epitaxial graphene/SiC

W. Jung,¹ D.-H. Oh,¹ I. Song,¹ H.-C. Shin,¹ S. J. Ahn,¹ Y. Moon,¹ C.-Y. Park,^{1,a)} and J. R. Ahn^{1,2,b)}

¹Department of Physics, Sungkyunkwan University, Suwon 440-746, South Korea

²SAINT, Sungkyunkwan University, Suwon 440-746, South Korea

(Received 11 June 2014; accepted 12 August 2014; published online 21 August 2014)

We demonstrate that molecular ordering of pentacene (Pn) on graphene depends on the interaction between graphene and its underlying SiC substrate. The adsorption of Pn molecules on zero-layer (ZL) and single-layer (SL) graphene, which were grown on a Si-faced 6H-SiC(0001) wafer, was studied using scanning tunneling microscopy (STM). Pn molecules form a quasi-amorphous layer on ZL graphene, which interacts strongly with the underlying SiC substrate. In contrast, they form a uniformly ordered layer on the SL graphene having a weak graphene-SiC interaction. Furthermore, we could change the configuration of Pn molecules on the SL graphene by using STM tips. The results suggest that the molecular ordering of Pn on graphene and the Pn/graphene interface structure can be controlled by a graphene-substrate interaction. © 2014 AIP Publishing LLC. [<http://dx.doi.org/10.1063/1.4893880>]

Graphene is an extraordinary material exhibiting unique physical properties that impart it with excellent prospects for a variety of applications.^{1–11} Among them, in the field of electronic devices, graphene has replaced electrode and/or channel parts to enhance device performances.^{8,10–13} For example, graphene was used as a channel material in a radio frequency field emission transistor (FET)⁹ and as an electrode material in a solar cell¹² and a light emission diode (LED).¹³ Furthermore, one of the technical advances in electronic devices has been the development of organic devices that are lighter, more flexible, and less expensive than inorganic devices.^{14,15} Therefore, it has only been logical to utilize graphene in organic devices such as organic FETs, solar cells, and LEDs.^{16–18} One of the key factors that determine the performance of organic devices is the interface structure between the organic molecules and the electrode materials.^{16–18} In the development of graphene-based organic devices, understanding and controlling the configuration of organic molecules on graphene is one of the essential focal points of research.^{16–18} Among the various organic materials, Pentacene (Pn) has been regarded as one of the most promising candidates for an organic FET because of its high carrier mobility, chemical stability, and compatibility with low-temperature Si fabrication processes.^{17,18} In earlier studies, gold was used as an electrode material in a Pn FET, but showed a significant charge-injection barrier because of an unfavorable interface dipole layer formation.^{17,18} In contrast to the gold electrode, when graphene was employed as the electrode of a Pn FET, a superior interface contact between graphene and Pn reduced the contact resistance and the charge-injection barrier height.^{17,18}

Therefore, it is necessary to understand and manipulate the interface structure between organic molecules and graphene, to enhance further the performance of graphene-

based organic devices. On metal substrates, it was reported that the orientation of a Pn molecule could depend on the electronic structure of the substrate, when Bi(001) and Au(111) surfaces were used as the substrate.¹⁹ For Pn on exfoliated single-layer (SL) and bilayer graphene on a silicon dioxide (SiO₂) film, it was reported that the activation energy for molecular aggregation depended on a water layer at the graphene/SiO₂ interface.²⁰ A systematic investigation is thus required to study molecular ordering of Pn on graphene with different atomic and/or electronic structures. An extreme case is to use metallic and insulating graphene. Both insulating and metallic graphene can be epitaxially grown on 6H-SiC(0001).^{3,5,7,21–23} Zero-layer (ZL) graphene on 6H-SiC(0001) has the same atomic structure as SL graphene but is insulating because most of the carbon atoms of the ZL graphene are covalently bonded to the Si atoms of the underlying SiC substrate.^{21,22} In contrast, SL graphene located on the ZL graphene is metallic, showing typical Dirac electron behavior.^{21,22}

Epitaxial graphene was grown on a Si-faced 6H-SiC(0001) wafer in an ultra-high vacuum (UHV) chamber with a base pressure of 5×10^{-11} Torr. The SiC wafer was hydrogen-etched in a separate chamber before the growth of graphene. The hydrogen-etched SiC wafer was then transferred to the UHV chamber and heated overnight to 600 °C to degas. The wafer was next exposed to Si flux, while being maintained at 850 °C, to remove native Si oxides. The ZL graphene was grown after heating the wafer to 1150 °C, whereas the SL graphene was grown after heating the wafer to 1200 °C. Pn in a graphite crucible was outgassed overnight in the UHV chamber. Pn flux was controlled by adjusting the temperature of the crucible. All Pn films on graphene in this report were grown at RT, where the pressure of the chamber was maintained below 2×10^{-10} Torr during the deposition of Pn. All STM images were acquired at RT using an Omicron VT-STM in constant current mode, where electrochemically etched tungsten tips were employed. A surface

^{a)}Electronic mail: cypark@skku.edu

^{b)}Electronic mail: jrahn@skku.edu

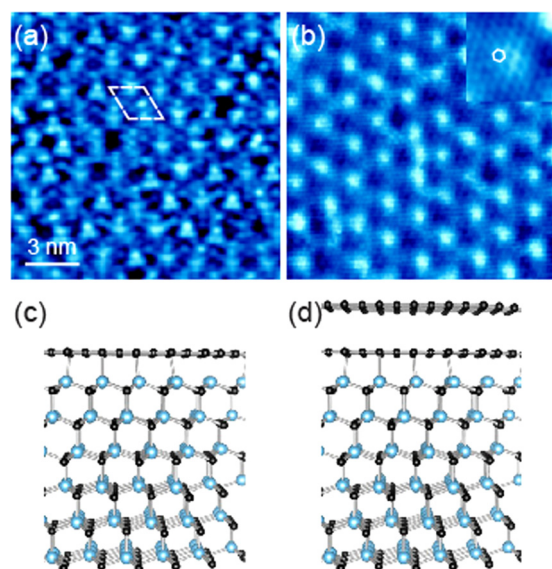


FIG. 1. STM images of (a) ZL graphene ($V_s = -1.5$ V, tunneling current (I_t) = 100 pA) and (b) SL graphene ($V_s = -0.1$ V, $I_t = 500$ pA). Dashed lines in (a) indicate the superstructure of the ZL graphene. The inset in (b) is an enlarged STM image, where the solid hexagon indicates the atomic hexagonal ring of graphene. Atomic structure models of (c) ZL and (d) SL graphene on 6H-SiC(0001), where blue and black spheres indicate Si and C atoms, respectively.

that is covered dominantly with the ZL (or SL) graphene can be produced.^{3,5,7,21,22} When only one of two kinds of graphene was used, it was not obvious whether the different growth mechanisms originate from the interaction between graphene and the substrate because other factors such as Pn flux can also be involved. Therefore, it was more efficient to use a surface covered with both ZL and SL graphene. In particular, Pn molecules were very mobile at low coverage on SL graphene so that when a surface covered with only SL graphene was used, it was very difficult to determine Pn coverage.

Figures 1(a) and 1(b) show STM images of the superstructures of the ZL and SL graphene, respectively. When a Si-faced 6H-SiC(0001) wafer was heated to 850 °C under Si flux, its surface reconstructed to a Si-terminated (3×3) phase.²⁴ The Si-terminated surface further reconstructed sequentially to and $(6\sqrt{3} \times 6\sqrt{3})R30^\circ$ when heating to higher temperatures.²⁴ The $(\sqrt{3} \times \sqrt{3})R30^\circ$ surface is another Si-terminated structure consisting of Si adatoms,

while the $(6\sqrt{3} \times 6\sqrt{3})R30^\circ$ surface is C-terminated.²⁴ The $(6\sqrt{3} \times 6\sqrt{3})R30^\circ$ superstructure is nothing but the ZL graphene having the same atomic structure as SL graphene, as shown in Figure 1(c).^{22,24} Most of the carbon atoms of the ZL graphene are covalently bonded to the Si atoms of the underlying SiC substrate, resulting in an insulating graphene, not showing Dirac electron behavior.^{22,24} The SiC wafer was heated to a higher temperature of 1200 °C to grow SL graphene, as displayed in Figure 1(b).²⁴ The SL graphene has a (6×6) superstructure and is located on the ZL graphene [Figure 1(d)].^{21,22,24} The SL graphene shows typical linear energy dispersions of Dirac electrons and is n-type because electrons are transferred to it from the SiC substrate.^{21,22,24}

Pn molecules were deposited on the ZL and SL graphene at RT. Figure 2(a) shows an STM image of Pn-covered ZL graphene at low Pn coverage. A “kidney bean”-like feature in Figure 2(a) represents a single Pn molecule lying flat, with the inset displaying the molecular structure of Pn overlapped with the “kidney bean” like feature. This feature of Pn in an STM image is consistent with STM images of Pn on other substrates.^{23,25,26} The image shows that the single Pn molecule has three preferential orientations, as indicated by yellow arrows, which is in accordance with STM experiments reported previously.²³ The existence of the three preferential orientations suggests there is a strong interaction between the ZL graphene and the single Pn molecule. In the ZL graphene [Figure 1(c)], there are two kinds of carbon atoms: one has an unsaturated π bond and the other has a saturated π bond.^{22,24} The carbon atoms with unsaturated π bonds may contribute to the adsorption of Pn on the ZL graphene because of their chemical reactivity, resulting in three preferential orientations of Pn following the structural symmetry of the ZL graphene, where the yellow hexagons indicate the $(6\sqrt{3} \times 6\sqrt{3})R30^\circ$ superstructure. When Pn coverage is increased, the molecules begin to pair, as indicated by dotted circles in Figure 2(b). The intermolecular distance of a Pn molecule pair was approximately 9.77 Å. The intermolecular distance is more than that found in a Pn bulk phase,²⁷ which suggests that the intermolecular interaction of Pn molecules on the ZL graphene is weaker than the interaction between Pn and the ZL graphene. At higher Pn coverage, the three preferential orientations of Pn molecules were maintained and the adsorbed molecules were not mobile at RT as a result of which the Pn molecules did not show any long-range order, as shown in Figure 2(c).

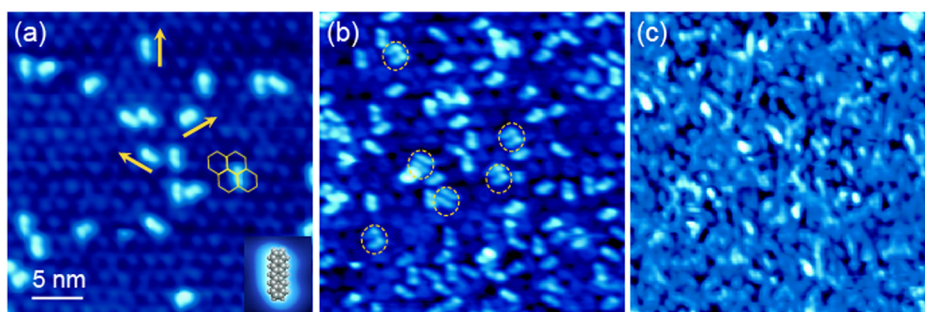


FIG. 2. STM images of Pn-covered ZL graphene with different Pn coverages. (a) An STM image ($V_s = -3.0$ V, $I_t = 100$ pA) with low Pn coverage, where yellow arrows indicate the molecular orientations of Pn, the yellow hexagons indicate the superstructure of the ZL graphene. (b) An STM image ($V_s = -2.1$ V, $I_t = 50$ pA) with intermediate Pn coverage, where the dotted yellow rings indicate Pn molecule pairs. (c) An STM image ($V_s = -2.1$ V, $I_t = 50$ pA) with high Pn coverage.

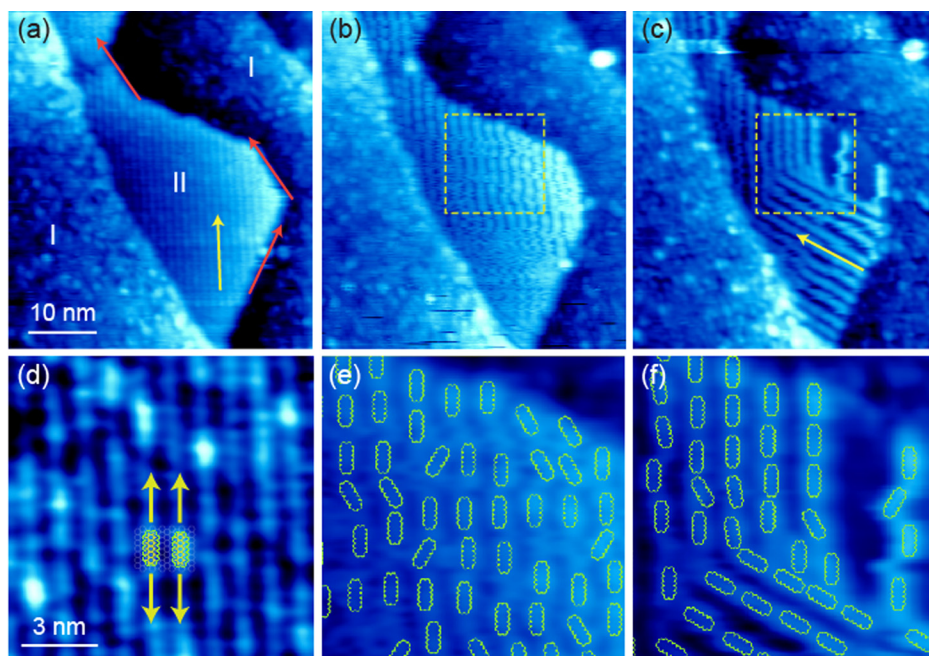


FIG. 3. (a)–(c) STM images of the first Pn layer on SL graphene. (a) An STM image of the saturated first Pn layer ($V_s = -2.7$ V, $I_t = 30$ pA), where I and II indicate the domains of the ZL and SL graphene, respectively, and the red and yellow arrows indicate the directions of the edge and the Pn molecule chain, respectively. (b) and (c) STM images ($V_s = -3.0$ V, $I_t = 30$ pA) acquired after removing Pn molecules by using an STM tip. (d)–(f) Enlarged STM images of (a), (b), and (c), respectively.

In contrast to the ZL graphene, the growth mechanism of Pn molecules on SL graphene was much different, as displayed in Figures 3 and 4. On the SL graphene, at low Pn coverage, single Pn molecules were not observed in the STM images at RT. The nonexistence of single Pn molecules in STM images does not imply that they were not adsorbed on the SL graphene because, at high coverage, Pn molecules were observed in the STM images. The nonexistence of single Pn molecules in STM images, thus, suggests that single Pn molecules are very mobile at RT on the SL graphene, as

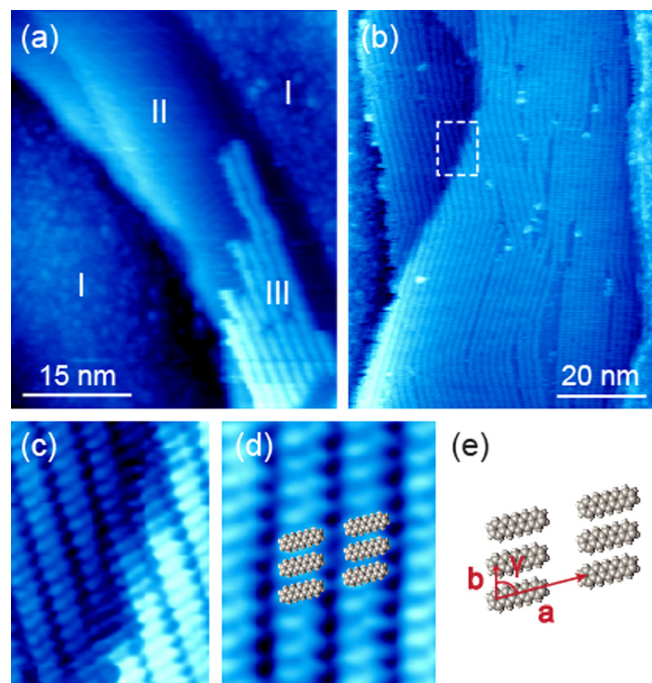


FIG. 4. (a) An STM image ($V_s = -3.0$ V, $I_t = 30$ pA) of the second Pn layer on SL graphene, where I, II, and III indicate Pn-covered ZL graphene and the first and the second Pn layers on SL graphene, respectively. (b) An STM image ($V_s = +1.6$ V, $I_t = 30$ pA) of the fully covered second Pn layer on SL graphene. (c) and (d) Enlarged STM images of (b). (e) The unit cell of the second Pn layer.

opposed to those on the ZL graphene. As mentioned before, however, single Pn molecules were observed on the ZL graphene at RT. The disparity in behavior of the Pn molecules at low and high coverages between the ZL and SL graphenes lead us to conclude that the interaction between Pn and SL graphene is much weaker than that between Pn and ZL graphene. When Pn molecules fully covered the SL graphene, resulting in the first Pn layer, they could be observed in the STM images [Figure 3(a)]. The domains of the ZL and SL graphene in Figure 3(a) are indicated by domains I and II, respectively. The domains can be clearly determined because the configurations of Pn molecules are much different from each other: Pn molecules are disordered in domain-I but show long-range order in domain-II. The domains I and II can be thus assigned to ZL and SL graphene, respectively. The configuration of Pn molecules on the SL graphene (domain-II) resembles an array of linear molecular chains, as seen in Figure 3(d), where the molecular structure of Pn is shown to overlap the enlarged STM image. In this configuration, the Pn molecules are orientated along the chain direction and the inter-chain distance is approximately 11.9° C. The preferential direction of the edges of the epitaxial graphene domains on 6H-SiC(0001) was reported to be the armchair direction,²⁸ while the graphene domains on metal substrates prefer zigzag edges.²⁹ The red arrows in Figure 3(a) indicate the armchair directions. The orientation of the Pn chains on the metallic SL graphene can thus be assigned a zigzag direction, as indicated by the yellow arrow in Figure 3(a).

Because of the weak interaction between Pn and SL graphene, we could remove Pn molecules at RT using an STM tip, as shown in Figures 3(b) and 3(c). In the course of repeated scanning with a bias voltage (V_s) of -2.7 V, Pn molecules were gradually removed. Interestingly, the Pn molecular chains experienced selective removal: every other Pn molecular chain was removed, as shown in Figure 3(b). As a result, the inter-chain distance of the Pn molecular chains increased from 11.9 to 19.2 Å. The selective removal of the

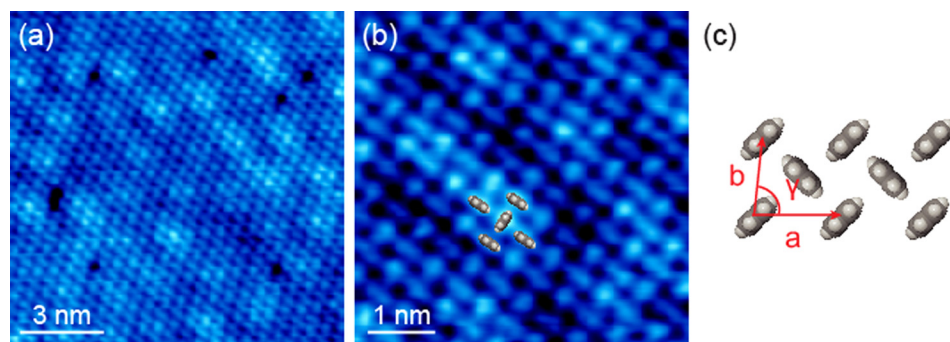


FIG. 5. (a) An STM image ($V_s = -1.6$ V, $I_t = 50$ pA) of a Pn film on SL graphene with Pn coverage of approximately 5 monolayer. (b) An enlarged STM image of (a). (c) The unit cell of the Pn film, where Pn molecules stand up.

molecules suggests there is another ordered phase of Pn molecules at a lower Pn coverage. The orientations of the Pn molecules were tilted at an angle in the molecular chains with the wider inter-chain distance, as shown in the enlarged STM image [Figure 3(e)]. The inter-chain distance of 19.2 \AA is similar to the size of the (6×6) unit cell of the SL graphene. The stability of the Pn molecular chains can therefore be related to an interaction between Pn and the superstructure of the SL graphene. In one case, we could even change the orientation of the molecular chains, as shown in Figure 3(c). The orientation of the lower Pn molecular chains was rotated by 60° , as indicated by the yellow arrow, while the upper chains maintained the same orientation. When the V_s was negative, the Pn desorption was enhanced. In particular, when the V_s was below -2.1 V, the Pn desorption was more frequently observed. In comparison to the negative V_s , when the V_s was positive, the Pn desorption was rarely observed. As described in Ref. 30, there are two kinds of interactions between an adsorbate and a STM tip. One is a van der Waals interaction without requiring an electric field and another is an electric field-induced charge redistribution. In this case, there exists dependence on an electric field induced by the V_s . Thus, the desorption and reorientation of Pn may be mainly induced by the electric-field-induced charge redistribution. The strength of a bond between Pn and graphene may be weakened by the charge redistribution resulting in the accumulation of electrons at an anti-bonding state.

After the first Pn layer fully covered the SL graphene, the second Pn layer began to grow, as can be seen in Figure 4. In Figure 4(a), domain-I indicates Pn-covered ZL graphene and domain-II and domain-III indicate the first and the second Pn layers on SL graphene, respectively. As described above, the domain of the Pn-covered ZL graphene can be clearly distinguished by the disordered configuration of Pn molecules (domain-I). Furthermore, the first Pn layer on SL graphene can be also ascertained by the linear chain configuration of Pn molecules (domain-II). However, this feature of the linear molecular chains was not as clearly visible as that observed before the growth of the second Pn layer. This may have been caused by the presence of mobile Pn molecules on the first Pn layer, during the growth of the second Pn layer. The second Pn layer (domain-III) began to grow from the edges of single-layer graphene domains [Figure 4(a)] and fully covered the first Pn layer [Figure 4(b)]. Interestingly, the second Pn layer grew continuously through step edges, as indicated by the dotted rectangle in Figure 4(b). The orientation of the Pn molecules in the second layer is similar to that of the first Pn layer on graphite.³¹ The Pn molecule is

tilted at an angle with respect to the chain direction [Figures 4(c) and 4(d)]. The unit cell of the second Pn layer is indicated in Figure 4(e). The inter-chain distance, indicated by a , is approximately 17.7 \AA and the intermolecular distance along the chain direction, indicated by b , is approximately 7.0 \AA , where the angle γ is approximately 73° .

Pn films have been grown at high pressure above 1×10^{-6} Torr and moderate temperatures above 100°C for device applications.^{17,18} When we assume the same flux of Pn, at the higher pressure, water molecules can degrade the quality of crystallinity of Pn films. The quality of the Pn films that were grown and observed in the STM experiments at ultra high vacuum may show the highest quality on each graphene layer, which may be degraded at higher pressure. On the other hand, the temperature can be an important factor. In general, annealing at higher temperatures can result in higher quality of crystalline. Thus, when a crystal can be grown at RT, the same crystal is observed at higher temperature if there is no phase transition at higher temperatures. In this sense, multilayer Pn films were grown on SL graphene at RT, as shown in Figure 5. The coverage of the Pn film is approximately 5 monolayer. The Pn film is crystalline and shows a typical herringbone structure of a Pn film, where the unit cell with $a = 6.1 \text{ \AA}$, $b = 6.1 \text{ \AA}$, and $\gamma = 84^\circ$ is shown in Figure 5(c). This result suggests that the same crystalline Pn film can be produced at higher temperatures. As expected, when the Pn film was annealed at 150°C , we did not find any significant change in STM images.

In conclusion, the effect of the atomic and/or electronic structures of graphene on the growth of Pn was studied using STM. Pn-graphene interaction was found to be strong when adsorbed on the ZL graphene but weak on the SL graphene. On the ZL graphene, there are preferential adsorption sites at which Pn molecules are immobile at RT. The immobile Pn molecules have local preferential orientations but do not show a long-range order. On the SL graphene, however, the Pn molecules are very mobile at RT, resulting in uniformly ordered Pn layers at high Pn coverage. Therefore, we suggest that the configuration of Pn molecules on graphene can be controlled by a graphene-substrate interaction.

This study was supported by a National Research Foundation of Korea (NRF) Grant (No. 2012R1A1A2041241).

¹K. S. Novoselov, A. K. Geim, S. V. Morozov, D. Jiang, M. I. Katsnelson, I. V. Grigorieva, S. B. Dubonos, and A. A. Firsov, *Nature* **438**, 197 (2005).
²Y. Zhang, Y.-W. Tan, H. L. Stormer, and P. Kim, *Nature* **438**, 201 (2005).

- ³T. Ohta, A. Bostwick, T. Seyller, K. Horn, and E. Rotenberg, *Science* **313**, 951 (2006).
- ⁴Y.-W. Son, M. L. Cohen, and S. G. Louie, *Nature* **444**, 347 (2006).
- ⁵A. Bostwick, T. Ohta, T. Seyller, K. Horn, and E. Rotenberg, *Nat. Phys.* **3**, 36 (2007).
- ⁶V. V. Cheianov, V. Falko, and B. L. Altshuler, *Science* **315**, 1252 (2007).
- ⁷S. Y. Zhou, G.-H. Gweon, A. V. Fedorov, P. N. First, W. A. de Heer, D.-H. Lee, F. Guinea, A. H. Castro Neto, and A. Lanzara, *Nature Mater.* **6**, 770 (2007).
- ⁸K. S. Kim, Y. Zhao, H. Jang, S. Y. Lee, J. M. Kim, K. S. Kim, J.-H. Ahn, P. Kim, J.-Y. Choi, and B. H. Hong, *Nature* **457**, 706 (2009).
- ⁹Y.-M. Lin, C. Dimitrakopoulos, K. A. Jenkins, D. B. Farmer, H.-Y. Chiu, A. Grill, and P. Avouris, *Science* **327**, 662 (2010).
- ¹⁰H. Yang, J. Heo, S. Park, H. J. Song, D. H. Seo, K.-E. Byun, P. Kim, I. Yoo, H.-J. Chung, and K. Kim, *Science* **336**, 1140 (2012).
- ¹¹J.-H. Lee, E. K. Lee, W.-J. Joo, Y. Jang, B.-S. Kim, J. Y. Lim, S.-H. Choi, S. J. Ahn, J. R. Ahn, M.-H. Park, C.-W. Yang, B. L. Choi, S.-W. Hwang, and D. Whang, *Science* **344**, 286 (2014).
- ¹²X. Wang, L. Zhi, and K. Müllen, *Nano Lett.* **8**, 324 (2008).
- ¹³J. Wu, M. Agrawal, H. A. Becerril, Z. Bao, Z. Liu, Y. Chen, and P. Peumans, *ACS Nano* **4**, 43 (2010).
- ¹⁴B.-G. Kim, E. J. Jeong, J. Chung, S. Seo, B. Koo, and J. Kim, *Nature Mater.* **12**, 659 (2013).
- ¹⁵Y. Diao, B. C.-K. Tee, G. Giri, J. Xu, D. H. Kim, H. A. Becerril, R. M. Stoltenberg, T. H. Lee, G. Xue, S. C. B. Mannsfeld, and Z. Bao, *Nature Mater.* **12**, 665 (2013).
- ¹⁶Y. Wen, J. Chen, L. Zhang, X. Sun, Y. Zhao, Y. Guo, G. Yu, and Y. Liu, *Adv. Mater.* **24**, 1471 (2012).
- ¹⁷W. H. Lee, J. Park, S. H. Sim, S. B. Jo, K. S. Kim, B. H. Hong, and K. Cho, *Adv. Mater.* **23**, 1752 (2011).
- ¹⁸S. Lee, G. Jo, S.-J. Kang, G. Wang, M. Choe, W. Park, D.-Y. Kim, Y. H. Kahng, and T. Lee, *Adv. Mater.* **23**, 100 (2011).
- ¹⁹G. E. Thayer, J. T. Sadowski, F. M. zu Heringdorf, T. Sakurai, and R. M. Tromp, *Phys. Rev. Lett.* **95**, 256106 (2005).
- ²⁰M. Chhikara, E. Pavlica, A. Matković, A. Beltaos, R. Gajic, and G. Bratina, *Carbon* **69**, 162 (2014).
- ²¹C. Jeon, H.-C. Shin, I. Song, M. Kim, J.-H. Park, J. Nam, D.-H. Oh, S. Woo, C.-C. Hwang, C.-Y. Park, and J. R. Ahn, *Sci. Rep.* **3**, 2725 (2013).
- ²²S. Kim, J. Ihm, H. J. Choi, and Y.-W. Son, *Phys. Rev. Lett.* **100**, 176802 (2008).
- ²³C. Shi, C. Wei, H. Han, G. Xingyu, Q. Dongchen, W. Yuzhan, and A. T. S. Wee, *ACS Nano* **4**, 849 (2010).
- ²⁴C. Riedl, C. Coletti, and U. Starke, *J. Phys. D: Appl. Phys.* **43**, 374009 (2010).
- ²⁵J. A. Smerdon, M. Bode, N. P. Guisinger, and J. R. Guest, *Phys. Rev. B* **84**, 165436 (2011).
- ²⁶H. G. Zhang, J. T. Sun, T. Low, L. Z. Zhang, Y. Pan, Q. Liu, J. H. Mao, H. T. Zhou, H. M. Guo, S. X. Du, F. Guinea, and H.-J. Gao, *Phys. Rev. B* **84**, 245436 (2011).
- ²⁷D. Nabok, P. Puschnig, C. Ambrosch-Draxl, O. Werzer, R. Resel, and D.-M. Smilgies, *Phys. Rev. B* **76**, 235322 (2007).
- ²⁸M. Ye, Y. T. Cui, Y. Nishimura, Y. Yamada, S. Qiao, A. Kimura, M. Nakatake, H. Namatame, and M. Taniguchi, *Eur. Phys. J. B* **75**, 31 (2010).
- ²⁹T. Ma, W. Ren, X. Zhang, Z. Liu, Y. Gao, L.-C. Yin, X.-L. Ma, F. Ding, and H.-M. Chenga, *Proc. Natl. Acad. Sci. U.S.A.* **110**, 20386 (2013).
- ³⁰P. Avouris, *Acc. Chem. Res.* **28**, 95 (1995).
- ³¹J. Götzen, D. Käfer, C. Wöll, and G. Witte, *Phys. Rev. B* **81**, 085440 (2010).